Isotopic constraints on heterogeneous sulfate production in Beijing haze

Pengzhen He[1], Becky Alexander[2], Lei Geng[1], Xiyuan Chi[1], Shidong Fan[1], Haicong Zhan[1], Hui Kang[1], Guangjie Zheng[3]†, Yafang Cheng[3,4], Hang Su[4,3], Cheng Liu[1,5,6], Zhouqing Xie[1,5,6]*

[1]Anhui Province Key Laboratory of Polar Environment and Global Change, School of Earth and Space Sciences, University of Science and Technology of China, Hefei, Anhui 230026, China.

[2]Department of Atmospheric Sciences, University of Washington, Seattle, WA 98195, USA.

[3]Multiphase Chemistry Department, Max Planck Institute for Chemistry, Mainz 55128, Germany.

[4]Jinan University, Institute for Environment and Climate Research, Guangzhou, Guangdong 511443, China.

[5]Key Lab of Environmental Optics and Technology, Anhui Institute of Optics and Fine Mechanics, Chinese Academy of Sciences, Hefei, Anhui 230031, China.

[6]Center for Excellence in Urban Atmospheric Environment, Institute of Urban Environment, Chinese Academy of Sciences, Xiamen, Fujian 361021, China.

**Corresponding to*: Zhouqing Xie (zqxie@ustc.edu.cn)

†: Now at: Atmospheric Sciences Division, Brookhaven National Laboratory, Upton, NY 11973, USA.

Abstract. Discerning mechanisms of sulfate formation during fine-particle pollution (referred to as haze hereafter) in Beijing is important for understanding the rapid evolution of haze and for developing cost-effective air pollution mitigation strategies. Here we present observations of the oxygen-17 excess of $PM_{2.5}$ sulfate ($\Delta^{17}O(SO_4^{2-})$) collected in Beijing haze from October 2014 to January 2015 to constrain possible sulfate formation pathways. Throughout the sampling campaign, the 12h-averaged $PM_{2.5}$ concentrations ranged from 16 to 323 μg m^{-3} with a mean of (141±88 (1σ)) μg m^{-3}, with SO_4^{2-} representing 8–25 % of $PM_{2.5}$ mass. The observed $\Delta^{17}O(SO_4^{2-})$ varied from 0.1 ‰ to 1.6 ‰ with a mean of (0.9±0.3) ‰. $\Delta^{17}O(SO_4^{2-})$ increased with $PM_{2.5}$ levels in October 2014 while the opposite trend was observed in November 2014 to January 2015. Our estimate suggested that in-cloud reactions dominated sulfate production in polluted days (PD, $PM_{2.5} \geq 75$ μg m^{-3}) of Case II in October 2014 due to the relatively high cloud liquid water content, with a fractional contribution up to 68 %. During PD of Case I and III–V, heterogeneous sulfate production (P_{het}) was estimated to contribute 41–54 % to total sulfate formation with a mean of (48±5) %. For the specific mechanisms of heterogeneous oxidation of SO_2, chemical reaction kinetics calculations suggested S(IV) (= $SO_2 H_2O + HSO_3^- + SO_3^{2-}$) oxidation by H_2O_2 in aerosol water accounted for 5–13 % of P_{het}. The relative importance of heterogeneous sulfate production by other mechanisms was constrained by our observed $\Delta^{17}O(SO_4^{2-})$. Heterogeneous sulfate production via S(IV) oxidation by O_3 was estimated to contribute 21–22 % of P_{het} on average. Heterogeneous sulfate production pathways that result in zero-$\Delta^{17}O(SO_4^{2-})$, such as S(IV) oxidation by NO_2 in aerosol water and/or by O_2 via a radical

chain mechanism, contributed the remaining 66–73 % of P_{het}. The assumption about the thermodynamic state of aerosols (stable or metastable) was found to significantly influence the calculated aerosol pH (7.6 ±0.1 or 4.7 ±1.1, respectively), and thus influence the relative importance of heterogeneous sulfate production via S(IV) oxidation by NO_2 and by O_2. Our local atmospheric conditions-based calculations suggest sulfate formation via NO_2 oxidation can be the dominant pathway in aerosols at high pH-conditions calculated assuming stable state while S(IV) oxidation by O_2 can be the dominant pathway providing that highly acidic aerosols (pH ≤ 3) exist. Our local atmospheric conditions-based calculations illustrate the utility of $\Delta^{17}O(SO_4^{2-})$ for quantifying sulfate formation pathways, but this estimate may be further improved with future regional modelling work.

1 Introduction

Frequent occurrence of haze events in Beijing and throughout the North China Plain (NCP) during cold seasons is a health threat for round 400 million people living there. High concentrations of $PM_{2.5}$ (particulate matter with an aerodynamic diameter less than 2.5 μm), of which the daily average can exceed 300 μg m^{-3} during severe haze (He et al., 2014; Jiang et al., 2015), contribute to cardiovascular morbidity and mortality (Brook et al., 2010; Cheng et al., 2013). As one of the major components of $PM_{2.5}$, sulfate is of particular concern due to its high concentrations in haze days (Zheng et al., 2015b; Zheng et al., 2015a) and its key role in the climate system (Seinfeld and Pandis, 2006). Hourly sulfate concentrations can exceed 100 μg m^{-3} and account for up to one quarter of $PM_{2.5}$ mass during severe haze (Zheng et al., 2015a). However, due to the generally low solar radiation and cloud liquid water content during haze (Zheng et al., 2015a; Wang et al., 2014), conventional sulfate formation via OH oxidation in the gas-phase and from aqueous-phase SO_2 (referred to as S(IV) = $SO_2 H_2O + HSO_3^- + SO_3^{2-}$) oxidation by H_2O_2 (McArdle and Hoffmann, 1983), O_3 (Hoffmann and Calvert, 1985), and O_2 via a radical chain mechanism initiated by transition metal ions (TMIs) in clouds (Ibusuki and Takeuchi, 1987; Alexander et al., 2009; Harris et al., 2013) cannot explain the observed high sulfate concentrations (Zheng et al., 2015a). To explain the observed high sulfate concentrations during haze in Beijing and NCP, recent studies have suggested that heterogeneous reactions on/in aerosols/aerosol water are potentially important (He et al., 2014; Hung and Hoffmann, 2015; Cheng et al., 2016; Wang et al., 2016; Zheng et al., 2015a; Zheng et al., 2015b; Wang et al., 2014). In particular, Zheng et al. (2015a) largely improved the underestimate of modelled sulfate concentrations in 2013 Beijing haze by using a relative humidity-dependent uptake coefficient (γ) of SO_2 on aerosols, without knowing the specific mechanisms of heterogeneous oxidation of SO_2. Calculations by Guo et al. (2017) suggest heterogeneous oxidation of SO_2 in Beijing maybe dominated by O_2 via a radical chain mechanism initiated by TMIs. Laboratory work has suggested SO_2 oxidation by O_3 on mineral dust is a significant pathway for sulfate production (Li et al., 2006), but its role in Beijing haze has not been determined. More recently, Hung and Hoffmann (2015) proposed that rapid S(IV) oxidation by O_2 via a radical chain mechanism on acidic microdroplets (pH ≤ 3) could be responsible

for heterogeneous sulfate production in Beijing haze, while Cheng et al. (2016) suggested that S(IV) oxidation by NO_2 (Lee and Schwartz, 1982; Clifton et al., 1988) in aerosol water could be important due to the high relative humidity and NO_2 mole fraction during severe haze in NCP. Due to the strong pH-dependence of SO_2 oxidation and the large variability of model calculated aerosol pH in Beijing haze (Cheng et al., 2016; Wang et al., 2016; Liu et al., 2017), the relative importance of heterogeneous SO_2 oxidation is difficult to constrain.

The oxygen-17 excess ($\Delta^{17}O$) of sulfate, defined as $\Delta^{17}O = \delta^{17}O - 0.52\delta^{18}O$, wherein $\delta = (R_{sample}/R_{reference} - 1)$ with R representing the isotope ratios of $^{17}O/^{16}O$ or $^{18}O/^{16}O$ in the sample and the reference Vienna Standard Mean Ocean Water, respectively (Matsuhisa et al., 1978), is a useful tool for estimating the relative importance of different sulfate formation pathways because each oxidant transfers its $\Delta^{17}O$ signature to the product (Table 1) through SO_2 oxidation (Savarino et al., 2000). SO_2 has $\Delta^{17}O = 0$ ‰ due to the rapid isotopic exchange with abundant vapour water whose $\Delta^{17}O$ is near 0 ‰ (Holt et al., 1981). S(IV) oxidation by H_2O_2 and O_3 leads to $\Delta^{17}O(SO_4^{2-}) = 0.7$ ‰ and 6.5 ‰, respectively, on the basis of $\Delta^{17}O(H_2O_2) = 1.4$ ‰ (Savarino and Thiemens, 1999) and assuming $\Delta^{17}O(O_3) = 26$ ‰ (Vicars and Savarino, 2014; Ishino et al., 2017). Other sources of sulfate exhibit $\Delta^{17}O(SO_4^{2-})$ at or near 0 ‰. Specifically, sulfate directly emitted from natural and anthropogenic sources or formed by OH and O_2 oxidation has $\Delta^{17}O(SO_4^{2-})$ values at or near 0 ‰ (Dubey et al., 1997; Luz and Barkan, 2005; Lee et al., 2002; Bao et al., 2000). Sulfate produced by NO_2 oxidation is suggested to occur either via a radical chain mechanism (Shen and Rochelle, 1998), via oxygen-atom transfer from OH^- (Clifton et al., 1988), or from O_2 based on experimental results of He et al. (2014), resulting in $\Delta^{17}O(SO_4^{2-}) = 0$ ‰. Once formed, atmospheric sulfate does not undergo further isotopic exchange, and $\Delta^{17}O(SO_4^{2-})$ will not be altered by mass-dependent processes such as deposition.

In this work, characteristics of $PM_{2.5}$ $\Delta^{17}O(SO_4^{2-})$ during haze events from October 2014 to January 2015 in Beijing are reported, contributions of O_3 and H_2O_2 oxidation in heterogeneous sulfate formation are quantified, and the roles of NO_2 and O_2 oxidation are explored.

2 Materials and Methods

2.1 Sampling and atmospheric observations

A high volume air sampler (model TH-1000C II, Tianhong Instruments Co., Ltd, China) with quartz microfiber filter (Whatman Inc., UK, pre-combusted at 450 °C for 4 h) was used to collect $PM_{2.5}$ samples at a flow rate of 1.05 m^3 min^{-1} from October 2014 to January 2015. The collections lasted for 12 h (08:00–20:00 LT or 20:00–08:00 LT) for each sample. The sample site is located on the rooftop of the First Teaching Building at the campus of University of the Chinese Academy of Sciences (40.41 °N, 116.68 °E, around 20 m from the ground) in Beijing, around 60 km northeast of downtown. Hourly $PM_{2.5}$ concentration, SO_2, NO_2 and O_3 mole fractions were observed at Huairou station (40.33 °N, 116.63 °E) by Beijing Municipal Environmental Monitoring Center, which is about 10 km from our aerosol sampling site. The mole fraction of atmospheric

H_2O_2 was not observed in our campaign, but long-term observations from March to November in Beijing shows a good correlation between H_2O_2 mole fraction and air temperature (T in ℃) according to $[H_2O_2]/(\text{nmol mol}^{-1}) = 0.1155e^{0.0846T/℃}$. (Fu, 2014). In the present study, H_2O_2 mole fraction was estimated from our measured T with the above empirical equation. Our calculated H_2O_2 mole fraction based on this formula in October and November 2014 is respectively (0.32 ±0.08) nmol mol^{-1} and (0.17 ±0.04) nmol mol^{-1}, comparable to the observed values of (0.44 ±0.18) nmol mol^{-1} and (0.38 ±0.11) nmol mol^{-1}, respectively in October and November 2013 (Fu, 2014). Meteorological data including temperature, pressure and relative humidity were recorded by an automatic weather station (model MetPak with integrated wind sonic, Gill Instruments Limited, UK). Time reported in this paper is local time (LT = UTC + 8).

2.2 Measurements of ions and isotope ratios

The measurements of ions were conducted in Anhui Province Key Laboratory of Polar Environment and Global Change in the University of Science and Technology of China. A detailed description of the method for chemical analysis of NH_4^+, K^+, Ca^{2+}, Na^+, Mg^{2+}, SO_4^{2-}, NO_3^- and Cl^- can be found in the literature (Ye et al., 2015). Briefly, ions were extracted from a part (2 cm × 2 cm) of each filter with 20 ml of Millipore water (≥ 18 MΩ) by sonication for 80 min in an ice water bath. Insoluble substances in the extract were filtered with 0.45 μm filters before analysis. The pH of filtrates was measured by an ion activity meter (model PXS-215, Shanghai INESA Scientific Instrument Co., Ltd., China). And the ion concentrations were analysed using Dionex ICS-2100 ion chromatograph system (Thermo Fisher Scientific Inc., USA). Typical analytical precision by our instrument is better than 10 % RSD (relative standard deviation) for all ions (Chen et al., 2016). The preparation and measurements of $\Delta^{17}O(SO_4^{2-})$ were conducted in Isolab (https://isolab.ess.washington.edu/isolab/) at the University of Washington, USA. A detailed description of the method can be found in the literature (Savarino et al., 2001; Geng et al., 2013; Chen et al., 2016; Alexander et al., 2012). Briefly, $PM_{2.5}$ sample filters were dissolved in Millipore water (≥ 18 MΩ) and the insoluble substances were filtered. Pre-packed ion capture cartridges (Alltech Maxi-Clean IC-RP SPE) were used for the first step of removal of organics. Cations in the samples were replaced with sodium using a cation exchange resin and 30 % H_2O_2 solution was added as the second step of removal of organics. Excess H_2O_2 was removed via evaporation and SO_4^{2-} was separated from other anions (e.g., NO_3^-) by ion chromatography. After ion separation, SO_4^{2-} was converted to Ag_2SO_4, dried, and then pyrolyzed at 1000 °C in an elemental analyzer to form Ag(s), SO_2(g), and O_2(g). The produced gases were carried by He gas to pass through a liquid nitrogen trap to remove SO_2, and then a GC to further purify the O_2 gas which was finally induced to a mass spectrometer (Thermo Scientific MAT 253). Masses of 32, 33 and 34 of O_2 were measured to determine $\delta^{17}O$ and $\delta^{18}O$ and then $\Delta^{17}O$ was calculated. The typical amount of O_2 for each run is 0.4–0.8 μmol. The precision of $\Delta^{17}O$ measurements in our method is ±0.3 ‰ based on replicate analysis of standards, which is consistent with previous studies (Alexander et al., 2005; Sofen et al., 2014; Chen et al., 2016). To quantify the uncertainty in each sample, 30 samples were measured in triplicate, 2 samples in quadruplicate, and 2 samples in duplicate depending on the limitation of sample size. In

total, 10 filters sampled in non-polluted days (NPD, $PM_{2.5}$ < 75 μg m^{-3}) and 24 filters sampled in polluted days (PD, $PM_{2.5}$ ≥ 75 μg m^{-3}) were analysed.

2.3 Estimate of the overall rate of heterogeneous sulfate production

Heterogeneous sulfate production (P_{het}) is commonly parameterized in models according to Eq. (1) (Jacob, 2000; Zheng et al., 2015a):

$$P_{het} = \frac{3600\ s\ h^{-1} \times 96\ g\ mol^{-1} \times p}{RT}\left(\frac{R_p}{D_g} + \frac{4}{v\gamma}\right)^{-1} S_p[SO_2(g)] \quad (1)$$

where P_{het} is in unit of μg m^{-3} h^{-1}, 3600 s h^{-1} is a time conversion factor, 96 g mol^{-1} is the molar mass of SO_4^{2-}, p is atmospheric pressure in kPa, R is the gas constant (8.31 Pa m^3 mol^{-1} K^{-1}), and T is temperature in K. R_p is the radius of aerosol particles (m), D_g is the gas-phase molecular diffusion coefficient of SO_2 (m^2 s^{-1}), v is the mean molecular speed of SO_2 (g) (m s^{-1}), γ is the uptake coefficient of SO_2 on aerosols with the unit of 1, [SO_2 (g)] is the gas-phase mole fraction of SO_2 (nmol mol^{-1}) and S_p is the aerosol surface area per unit volume of air (m^2 m^{-3}). The typical tropospheric value of D_g and v is 2×10^{-5} m^2 s^{-1} and 300 m s^{-1}, respectively (Jacob, 2000). Observations of $PM_{2.5}$ mass concentrations ($c(PM_{2.5})$, μg m^{-3}) and $PM_{2.5}$ mean radius (m) during Beijing haze roughly follows an empirical formula: $R_p/m = (0.254c(PM_{2.5})/(\mu g\ m^{-3}) + 10.259)\times10^{-9}$ (Guo et al., 2014). By using the volume and surface area formulas of a sphere and the mean density of particles $\rho = 1.5\times10^6$ g m^{-3} (Guo et al., 2014), S_p can be estimated from Eq. (2). A relative humidity-dependent γ (= (2–5)$\times10^{-5}$, Eq. (3)) derived from Zheng et al. (2015a) during 2013 Beijing haze was used. This range of γ is also consistent with the estimated values of γ from $(1.6\pm0.7)\times10^{-5}$ to $(4.5\pm1.1)\times10^{-5}$ by Wang et al. (2016).

$$S_p = \frac{c(PM_{2.5})\times10^{-6}\ g\ \mu g^{-1}}{4/3\times\pi R_p{}^3\times\rho} \times 4\pi R_p{}^2 \quad (2)$$

$$\gamma = \begin{cases} 2\times10^{-5}, \Psi \le 50\ \% \\ 2\times10^{-5} + \frac{5\times10^{-5}-2\times10^{-5}}{100\%-50\%} \times (\Psi - 50\%), \ 50\ \% \le \Psi \le 100\ \% \end{cases} \quad (3)$$

where Ψ refers to relative humidity with the unit of %.

2.4 Estimate of primary sulfate

The primary sulfate, which is directly emitted into air, includes the sea salt source, terrigenous source and anthropogenic source (Li et al., 2013; Faloona, 2009). The concentration of sea salt sulfate was calculated by using the observed concentrations of Na^+ and the mass ratio of $c(SO_4^{2-})/c(Na^+)$ = 0.252 in seawater (Calhoun et al., 1991). The terrigenous sulfate was estimated using the observed concentrations of Ca^{2+} and the mass ratio of $c(SO_4^{2-})/c(Ca^{2+})$ = 0.18 in soil (Legrand et al., 1997), where $c(Ca^{2+})/c(Na^+)$ = 0.038 in seawater was used to calculate the fraction of observed Ca^{2+} from soil (Legrand and Mayewski, 1997). The anthropogenic primary sulfate is estimated as 3 % of anthropogenic SO_2 emissions in models (Faloona, 2009; Alexander et al., 2009). Supposing all the observed mole fraction of SO_2 and precursors of secondary sulfate are

anthropogenic, we have $c(ap)/96 = 0.03(c(SO_2)/64 + c(sas)/96)$, where $c(sas) = c(tos)–c(ss)–c(ts)–c(ap)$ and $c(ap)$, $c(sas)$, $c(tos)$, $c(ss)$ and $c(ts)$ is the mass concentrations of anthropogenic primary sulfate (ap), secondary sulfate (sas), total sulfate (tos), sea salt sulfate (ss) and terrigenous sulfate (ts). The estimated concentration of total primary sulfate ($p\text{-}SO_4^{2-}$) is the sum of primary sulfate from all these sources.

2.5 Estimate of sulfate production rate from OH oxidation in the gas-phase

The sulfate production rate from OH oxidation in the gas-phase (P_{SO2+OH}) can be expressed as:

$$P_{SO_2+OH} = \frac{3600\ s\ h^{-1} \times 96\ g\ mol^{-1} \times p \times R_{SO_2+OH}}{RT} \quad (4)$$

where P_{SO2+OH} is in unit of μg m^{-3} h^{-1}, 3600 s h^{-1}, 96 g mol^{-1}, p, R and T is the same as Eq. (1). R_{SO2+OH} is the chemical reaction rate (nmol mol^{-1} s^{-1}), calculated as shown in Table S1 and S2.

2.6 Estimate of in-cloud sulfate production rate

The main in-cloud sulfate formation pathways considered here include S(IV) oxidation by H_2O_2, O_3, NO_2 (Wang et al., 2016) and O_2 via a radical chain mechanism initiated by TMIs (Alexander et al., 2009). Their chemical reaction rate expressions ($R_{S(IV)+oxi}$) and rate constants (k) are summarized in Table S3. The rate of in-cloud sulfate production by a certain oxidant ($P_{cloud,\ S(IV)+oxi}$) can be expressed as (Seinfeld and Pandis, 2006):

$$P_{cloud,S(IV)+oxi} = 3600\ s\ h^{-1} \times 96\ g\ mol^{-1} \times L_c \times R_{S(IV)+oxi} \quad (5)$$

where $P_{cloud,\ S(IV)+oxi}$ is in unit of μg m^{-3} h^{-1}, 3600 s h^{-1} and 96 g mol^{-1} is the same as Eq. (1), and $R_{S(IV)+oxi}$ is in unit of M s^{-1}. Cloud liquid water content (L_c, in unit of mg m^{-3}) was derived from a global reanalysis, GEOS-FP (https://gmao.gsfc.nasa.gov/products/). By summing in-cloud S(IV) oxidation by H_2O_2, O_3, NO_2 and O_2 initiated by TMIs up, we can get the total rate of in-cloud sulfate production (P_{cloud}).

2.7 Isotopic constraints on sulfate formation pathways

Since S(IV) oxidation by O_3 and H_2O_2 are the sole sources of non-zero $\Delta^{17}O(SO_4^{2-})$ (Table 1) (Savarino et al., 2000), the relative importance of different sulfate formation pathways can be calculated as follows (Alexander et al., 2012):

$$\Delta^{17}O_{obs} = (6.5‰ \times f_{S(IV)+O_3}) + (0.7‰ \times f_{S(IV)+H_2O_2}) + (0 \times f_{zero-\Delta^{17}O}) \quad (6)$$

where $f_{S(IV)+O3}$ and $f_{S(IV)+H2O2}$ are fractional contributions of S(IV) oxidation by O_3 and H_2O_2 to the observed sulfate, respectively, and $f_{zero\text{-}\Delta17O}$ represents fractional contribution of sulfate with zero-$\Delta^{17}O$ processes such as primary sulfate, secondary sulfate formed via OH oxidation, NO_2 oxidation, and O_2 oxidation. By using Eq. (6) and the definition $f_{S(IV)+O3} + f_{S(IV)+H2O2} + f_{zero\text{-}\Delta17O} = 1$, we have $f_{S(IV)+O3} = (\Delta^{17}O_{obs}–0.7‰ \times f_{S(IV)+H2O2})/6.5‰$ and $f_{zero\text{-}\Delta17O} = (6.5‰–\Delta^{17}O_{obs}–5.8‰ \times f_{S(IV)+H2O2})/6.5‰$. Since $f_{S(IV)+O3}$, $f_{S(IV)+H2O2}$, and $f_{zero\text{-}\Delta17O}$ should be in the range of 0 to 1 at the same time, $f_{S(IV)+H2O2}$ is

further limited to meet $f_{S(IV)+H2O2} < \min\{\Delta^{17}O_{obs}/0.7‰, (6.5‰-\Delta^{17}O_{obs})/5.8‰\}$. Therefore, possible range of $f_{S(IV)+O3}$ and $f_{zero\text{-}\Delta17O}$ can be obtained at different $f_{S(IV)+H2O2}$ assumptions.

In addition, as sulfate with non-zero $\Delta^{17}O(SO_4^{2-})$ is produced either via in-cloud reactions or via heterogeneous reactions or both, Eq. (6) can also be written as follows:

$$\Delta^{17}O_{obs} = f_{het} \times \Delta^{17}O_{het} + f_{cloud} \times \Delta^{17}O_{cloud} + f_{SO_2+OH} \times \Delta^{17}O_{SO_2+OH} + f_p \times \Delta^{17}O_p \quad (7)$$

where f_{het}, f_{cloud}, f_{SO2+OH} and f_p respectively represents the fractional contribution of heterogeneous sulfate production, in-cloud sulfate production, gas-phase sulfate production and primary sulfate to the observed sulfate. $f_p = c(p\text{-}SO_4^{2-})/c(SO_4^{2-})$, $f_{het} = \{P_{het}/(P_{het}+P_{cloud}+P_{SO2+OH})\} \times (1-f_p)$, $f_{cloud} = \{P_{cloud}/(P_{het}+P_{cloud}+P_{SO2+OH})\} \times (1-f_p)$ and $f_{SO2+OH} = \{P_{SO2+OH}/(P_{het}+P_{cloud}+P_{SO2+OH})\} \times (1-f_p)$. $\Delta^{17}O_{het}$, $\Delta^{17}O_{cloud}$, $\Delta^{17}O_{SO2+OH}$ and $\Delta^{17}O_p$ respectively represents $\Delta^{17}O$ of corresponding sulfate produced via above pathways. Both $\Delta^{17}O_{SO2+OH}$ and $\Delta^{17}O_p$ are equal to 0 ‰. $\Delta^{17}O_{cloud}$ can be calculated as shown in Eq. (8) as the lifetime of sulfate produced in clouds will not depend on the specific S(IV) oxidant.

$$\Delta^{17}O_{cloud} = \frac{6.5‰ \times P_{cloud,S(IV)+O_3} + 0.7‰ \times P_{cloud,S(IV)+H_2O_2}}{P_{cloud}} \quad (8)$$

2.8 Calculation of aerosol liquid water content, aerosol pH and ionic strength (I_s)

Aerosol liquid water content, aerosol pH and I_s was calculated by the ISORROPIA II model, which is a thermodynamic equilibrium model for NH_4^+-K^+-Ca^{2+}-Na^+-Mg^{2+}-SO_4^{2-}-NO_3^--Cl^--H_2O aerosols (Fountoukis and Nenes, 2007). The ISORROPIA II model can solve forward problems in which T, relative humidity and the concentrations of gas + aerosols are known (e.g., NH_3 + NH_4^+), and reverse problems in which T, relative humidity and the concentrations of aerosol (but not gas) species are known. We used the forward method to calculate aerosol liquid water content, aerosol pH and I_s as this method has been shown to best predict aerosol pH (Hennigan et al., 2015). The aerosol liquid water content, pH and I_s was first calculated in metastable mode (assuming that bulk aerosol solution is supersaturated), which is consistent with previous studies about Beijing haze (Liu et al., 2017; Guo et al., 2017). However, the work of Rood et al. (1989) in California, USA suggested that not all aerosols are in metastable state, even though the fractional occurrence of metastable aerosols increases with increasing relative humidity in urban sites (roughly following Eq. (9)). We also calculated the aerosol liquid water content, pH and I_s assuming stable mode (assuming that bulk aerosols crystallize once saturation is exceeded), which is consistent with Wang et al. (2016). The input of observed inorganic ion concentrations and meteorological parameters are summarized in Table S4. Since gaseous NH_3 was not measured in our campaign, we used the empirical equation $[NH_3]/(nmol\ mol^{-1}) = 0.34[NO_X]/(nmol\ mol^{-1}) + 0.63$, derived from observations of Meng et al. (2011) in Beijing winter, to estimate the NH_3 mole fraction. We used NO_2 mole fraction instead of NO_X as input due to the lack of NO_X observations in our study, which would give a lower end of NH_3 mole fraction. Given the importance of aerosol liquid water content for reaction rates and the fact that ISORROPIA II underestimates aerosol liquid water content at low relative humidity (Bian et al., 2014), samples with relative humidity < 40 %

are excluded from analysis (Hennigan et al., 2015). This excludes 8 out of the total 34 samples (24 %), with 6 of them in NPD. A total of 4 samples in NPD and 22 samples in PD were analysed for aerosol liquid water content, aerosol pH and I_s. Due to that the predicted I_s is high (I_s > 10 M, Table S4), which suggests aerosol water is non-ideal, the influence of I_s on reaction rate constants (Table S3) and effective Henry's law constants (Table S5) is taken into consideration when the influence is known.

$$x(\text{metastable}) = \begin{cases} 0, & \Psi < 30\ \% \\ -0.024(\Psi/\%)^2 + 4.18\Psi/\% - 89.13, & 30\ \% \le \Psi \le 80\ \% \\ 100\ \%, & 80\ \% < \Psi \le 100\ \% \end{cases} \quad (9)$$

where x(metastable) is the fraction of metastable aerosols to total aerosols in the unit of %.

2.9 Estimate of aqueous concentrations of trace species

The aqueous concentrations of SO_2, O_3, H_2O_2 and NO_2 were calculated as described in Table S5. The determination of in-cloud concentrations of TMIs (here only Fe(III) and Mn(II) (Alexander et al., 2009)) is described below.

The concentration of soluble Fe(III) follows Eqs. (10)–(13) (Liu and Millero, 1999):

$$\log_{10}([\text{Fe(III)}]/c^{\ominus}) = \log_{10}(K^*_{\text{Fe(OH)}_3}(c^{\ominus})^2) + 3\log_{10}([\text{H}^+]/c^{\ominus}) + \log_{10}\left(1 + \beta_1^*([\text{H}^+]/c^{\ominus})^{-1} + \beta_2^*([\text{H}^+]/c^{\ominus})^{-2}\right) \quad (10)$$

where

$$\log_{10}(K^*_{\text{Fe(OH)}_3}(c^{\ominus})^2) = -13.486 - 0.1856(I_s/c^{\ominus})^{0.5} + 0.3073(I_s/c^{\ominus}) + 5254\text{K}/T \quad (11)$$

$$\log_{10}(\beta_1^*/(c^{\ominus})^2) = 2.517 - 0.8885(I_s/c^{\ominus})^{0.5} + 0.2139(I_s/c^{\ominus}) - 1320\text{K}/T \quad (12)$$

$$\log_{10}(\beta_2^*/(c^{\ominus})^2) = 0.4511 - 0.3305(I_s/c^{\ominus})^{0.5} - 1996\text{K}/T \quad (13)$$

and [Fe(III)] is the aqueous concentration of Fe(III) in unit of M, T is temperature in unit of K, and I_s is ionic strength in unit of M, $K^*_{\text{Fe(OH)3}}$ is the solubility product constant of $Fe(OH)_3$ in the unit of $(\text{mol L}^{-1})^{-2}$, and β^*_1 and β^*_2 is respectively first-order and second-order cumulative hydrolysis constants of Fe^{3+} in the unit of $(\text{mol L}^{-1})^2$.

Our calculation suggested in-cloud [Fe(III)] was in the range of 0.6 to 6.1 μM with a mean of (2.6±1.8) μM, which is similar to the observed values in NCP (Guo et al., 2012; Shen et al., 2012). The concentration of soluble Mn(II) in cloud water was set to be 1 μM in the present study, which is the general value observed in cloud water in NCP (Guo et al., 2012; Shen et al., 2012).

2.10 Estimate of sulfate production rate in aerosol water

The reaction rate expressions, rate constants (k) and the influence of I_s on k for sulfate production in aerosol water are summarized in Table S3. The overall rates for S(IV) oxidation in aerosol water depend not only on chemical reaction rates (Table S3) but also on mass transport limitations. A standard resistance model was used to estimate effects of mass transport following the work of Cheng et al. (2016):

$$\frac{1}{R_{\text{H,S(IV)+oxi}}} = \frac{1}{R_{\text{S(IV)+oxi}}} + \frac{1}{J_{\text{aq,lim}}} \quad (14)$$

where $R_{H,\,S(IV)+oxi}$ is the overall reaction rate for S(IV) oxidation by a certain oxidant (oxi) such as O_3, H_2O_2, NO_2 and O_2 on acidic microdroplets (M s^{-1}), $R_{S(IV)+oxi}$ is the chemical reaction rate (M s^{-1}) and $J_{aq,\,lim}$ is the rate limited by mass transfer from the gas to the aqueous phase (M s^{-1}). Due to the large decrease in the aqueous-phase reaction rate constant for TMI-initiated S(IV) oxidation by O_2 with increasing I_s (Martin and Hill, 1967) and the high I_s of aerosols (Table S4), combined with the fact that the rate constant for the S(IV) + O_2 mechanism on acidic microdroplets proposed by Hung and Hoffman (2015) likely includes the effect of TMIs, we do not directly consider TMI-initiated S(IV) oxidation by O_2 in aerosol water. $R_{S(IV)+oxi}$ was calculated as described in Table S3. The limiting mass transfer $J_{aq,\,lim}$ was calculated by Eqs. (15) and (16).

$$J_{aq,lim} = \min\{J_{aq}(SO_2), J_{aq}(oxi)\} \quad (15)$$

$$J_{aq}(X) = k_{MT}(X) \times [X(aq)] \quad (16)$$

where X = SO_2, O_3, H_2O_2 or NO_2 and k_{MT} (s^{-1}) is the mass transfer rate coefficient and was calculated as Eq. (17) (Cheng et al., 2016; Seinfeld and Pandis, 2006):

$$k_{MT}(X) = \left[\frac{R_p^2}{3D_g} + \frac{4R_p}{3\alpha v}\right]^{-1} \quad (17)$$

where R_p, D_g and v are the same as Eq. (1). The α used in our calculation is respectively 0.11 for SO_2, 0.23 for H_2O_2, 2.0×10^{-3} for O_3 and 2.0×10^{-4} for NO_2 (Seinfeld and Pandis, 2006; Jacob, 2000). The term on the left hand side of Eq. (17) is the gas-phase diffusion limitation while the term on the right hand side of Eq. (17) is the interfacial mass transport limitation. k_{MT} was limited by interfacial mass transport in our study.

The rate of heterogeneous sulfate production by a certain oxidant ($P_{het,\,S(IV)+oxi}$) in aerosol water can be expressed as:

$$P_{het,S(IV)+oxi} = 3600\ s\ h^{-1} \times 96\ g\ mol^{-1} \times L_a \times R_{H,S(IV)+oxi} \quad (18)$$

where $P_{het,\,S(IV)+oxi}$ is in the unit of μg m^{-3} h^{-1}, 3600 s h^{-1} and 96 g mol^{-1} is the same as Eq. (1). L_a is aerosol liquid water content in the unit of mg m^{-3} and $R_{H,\,S(IV)+oxi}$ is in the unit of M s^{-1}.

3 Results and Discussion

3.1 Characteristics of haze events in Beijing

Figure 1a shows the temporal evolution of concentrations of $PM_{2.5}$ and SO_4^{2-} during our sampling period. The 12h-averaged $PM_{2.5}$ concentrations ranged from 16 to 323 μg m^{-3} with a mean of (141±88 (1σ)) μg m^{-3}. In comparison, the Grade II of the Chinese National Ambient Air Quality Standard of daily $PM_{2.5}$ is 75 μg m^{-3}. The SO_4^{2-} concentrations varied from 1.5 to 56.4 μg m^{-3} with a mean of (21.2±15.4) μg m^{-3}. As shown in Fig. 1a, SO_4^{2-} concentrations presented a similar temporal trend as $PM_{2.5}$ concentrations, i.e., increased from a mean of (3.9±1.8) μg m^{-3} in non-polluted days (NPD, $PM_{2.5}$ < 75 μg m^{-3}) to (28.4±12.5) μg m^{-3} in polluted days (PD, $PM_{2.5}$ ≥ 75 μg m^{-3}). The fraction of SO_4^{2-} to $PM_{2.5}$ mass concentration ranged from 8–25 %, and increased from a mean of (11±2) % in NPD to (15±5) % in PD. The sulfur oxidation ratio (SOR, which equals to SO_4^{2-} molar concentration divided by the sum of SO_4^{2-} and SO_2 molar concentration), a proxy for

secondary sulfate formation (Sun et al., 2006), also increased rapidly with $PM_{2.5}$ levels, from a mean of 0.12 ±0.04 in NPD to 0.41 ±0.17 in PD (Fig. 1b).

Observed $\Delta^{17}O(SO_4^{2-})$ ($\Delta^{17}O_{obs}$) ranged from 0.1 ‰ to 1.6 ‰ with a mean of (0.9±0.3) ‰ (Fig. 1b). The highest $\Delta^{17}O_{obs}$ = 1.6 ‰ occurred during PD of Case II in October 2014 while the lowest $\Delta^{17}O_{obs}$ = 0.1 ‰ occurred during PD of Case IV in December 2014. $\Delta^{17}O_{obs}$ reported here is similar in magnitude to previous observations of $\Delta^{17}O(SO_4^{2-})$ in aerosols and rainwater collected in China (Lin et al., 2017; Li et al., 2013) and other mid-latitude sites (Table S6). The overall $\Delta^{17}O_{obs}$ levels during our entire sampling time are similar for NPD and PD, being (0.9±0.1) ‰ and (0.9±0.4) ‰, respectively. However, the NPD to PD difference of $\Delta^{17}O_{obs}$ can be case-dependent. For Case I and II in October 2014, $\Delta^{17}O_{obs}$ increased from NPD to PD, while the opposite trend was observed for Case III to V in November 2014 to January 2015 (Fig. 1b). These $\Delta^{17}O_{obs}$ variations are generally similar to variability in mole fractions of observed O_3 and calculated H_2O_2 (Fig. 1c), which is consistent with the fact that O_3 and H_2O_2 are the sole sources of non-zero $\Delta^{17}O(SO_4^{2-})$ (Table 1).

3.2 Direct estimate of sulfate formation pathways based on $\Delta^{17}O_{obs}$

Figure 2 shows the calculated possible fractional contributions of each formation pathway ($f_{S(IV)+H2O2}$, $f_{S(IV)+O3}$, and $f_{zero\text{-}\Delta17O}$) for each sample using Eq. (6). On average over all samples collected, $f_{S(IV)+O3}$ = 4–13 %, $f_{S(IV)+H2O2}$ = 0–88 %, and $f_{zero\text{-}\Delta17O}$ = 8–87 %. For samples during PD of Case IV in December 2014 with the three lowest $\Delta^{17}O_{obs}$ values (Fig. 1b), $f_{zero\text{-}\Delta17O}$ was respectively in the range of 57–95 %, 86–98 % and 57–95 %, corresponding to $f_{S(IV)+H2O2}$ being in the range of 0–43 %, 0–14 % and 0–43 % respectively, which clearly suggests zero-$\Delta^{17}O$ pathways dominated sulfate formation during PD of Case IV. However, for other samples, the maximum possible $f_{S(IV)+H2O2}$ ranged from 71 % to 100 % with a mean of (93 ±7) % while the maximum possible $f_{zero\text{-}\Delta17O}$ was 75 % to 92 % with a mean of (86 ±4) %, implying that sulfate formation during these sampling periods were dominated by H_2O_2 oxidation and/or zero-$\Delta^{17}O$ pathways.

3.3 Chemical kinetic calculations with the constraint of $\Delta^{17}O_{obs}$

The good correlation between relative humidity and SOR in Fig. 3a ($r = 0.76$, $p < 0.01$) suggests heterogeneous reactions played an important role in sulfate formation. Our local atmospheric conditions-based calculations show that overall heterogeneous sulfate production (P_{het}, see Sect. 2.3) presented similar trends with SO_4^{2-} concentrations except for Case II (Fig. 3b) and increased from a mean of (0.6±0.3) μg m^{-3} h^{-1} in NPD to (2.0±1.1) μg m^{-3} h^{-1} in PD during our entire sampling period. In comparison, Cheng et al. (2016) reported that the missing sulfate production rate required to explain the observed sulfate concentration is around 0.07 μg m^{-3} h^{-1} when $PM_{2.5}$ < 50 μg m^{-3} and around 4 μg m^{-3} h^{-1} when $PM_{2.5}$ > 400 μg m^{-3} during 2013 Beijing haze. We also calculated the contribution from primary sulfate and performed chemical kinetic calculations including SO_2 oxidation by OH in the gas-phase and in-cloud sulfate production (Fig. 4 and Table 2, see Sect. 2.4–2.6) to estimate the relative importance of heterogeneous sulfate production in our sampling period. Heterogeneous

reactions were found to contribute 41–54 % to total sulfate formation during PD of Case I and III–V, with a mean of (48±5) % (Fig. 4). This is consistent with Zheng et al. (2015a) who modelled that about half of the observed sulfate was from heterogeneous reactions during 2013 Beijing haze. In contrast, we found that during PD of Case II in October 2014, heterogeneous sulfate production only accounted for 23 % of total sulfate production while in-cloud sulfate production predominated total sulfate production with an estimated fraction of 68 %. The predominant role of in-cloud sulfate production in PD of Case II was supported by the relative high cloud liquid water content during this time period (Fig. 5a). Our local atmospheric conditions-based calculations also suggest the in-cloud sulfate production was dominated by H_2O_2 oxidation throughout our sampling period (Fig. 5b), which is consistent with previous findings that H_2O_2 oxidation is the most important in-cloud sulfate production pathway globally (Alexander et al., 2012) and in NCP (Shen et al., 2012). In addition, the $\Delta^{17}O$ of sulfate produced in clouds ($\Delta^{17}O_{cloud}$) was estimated to range from 0.5 ‰ to 0.8 ‰ with a mean of (0.6±0.1) ‰ during our sampling period and showed similar variations with $\Delta^{17}O_{obs}$ (Fig. 5c). The mean value of $\Delta^{17}O_{cloud}$ calculated here is close to $\Delta^{17}O(SO_4^{2-})$ in rainwater observed in central China (0.53±0.19 ‰) (Li et al., 2013) and at Baton Rouge, USA (0.62±0.32 ‰) (Jenkins and Bao, 2006). In addition, by using Eq. (7), the $\Delta^{17}O$ of sulfate produced via heterogeneous reactions ($\Delta^{17}O_{het}$) was calculated to be respectively 1.8 ‰, 3.1 ‰, 1.4 ‰, 0.1 ‰ and 0.8 ‰ for PD of Case I–V. Since $\Delta^{17}O(SO_4^{2-})$ produced via H_2O_2 oxidation is 0.7 ‰, smaller than $\Delta^{17}O_{het}$ in Case I–III and V, O_3 oxidation must contribute to heterogeneous sulfate production.

To explore the specific mechanisms of heterogeneous oxidation of SO_2, we calculated aerosol parameters such as aerosol liqiud water content, pH and ionic strength (I_s) by using the ISORROPIA II thermodynamic model (Fountoukis and Nenes, 2007) (Fig.6, see Sect. 2.8). It was found that the assumptions about aerosol thermodynamic state (salts crystallize once saturation is exceeded, termed as "stable state" or aerosol solution is supersaturated, termed as "metastable state") significantly influence the calculated aerosol pH, but have little impact on the calculated aerosol liqiud water content and I_s (Fig. 6). Calculated aerosol liqiud water content increased with $PM_{2.5}$ concentrations, from (5.3±7.4) μg m^{-3} in NPD to (63.5±54.6) μg m^{-3} in PD when assuming stable state and from (9.6±6.0) μg m^{-3} in NPD to (84.2±49.2) μg m^{-3} in PD when assuming metastable state (Fig. 6a). Calculated I_s was similar for stable and metastable assumptions, ranging from 11.3 to 51.6 M (Fig. 6b). The high I_s suggested aerosol water was non-ideal and thus the influence of I_s on reaction rate constants (Table S3) and effective Henry's law constants (Table S5) was taken into consideration when the influence is known. The bulk aerosol pH predicted in stable state was in the range of 7.5 to 7.8 with a mean of 7.6±0.1, consistent with bulk aerosol pH = 7.63±0.03 calculations during a haze event in Beijing 2015 predicted by Wang et al. (2016). The bulk aerosol pH calculated assuming metastable state was in the range of 3.4 to 7.6 with a mean of 4.7±1.1, consistent with the mean value of 4.2 calculated in metastable aerosol assumption during severe haze in Beijing 2015–2016 by Liu et al. (2017). The calculated aerosol pH assuming metastable state decreased with increasing $PM_{2.5}$ levels, from a mean of 6.5±1.3 in NPD to 4.4±0.6 in PD, while that assuming stable state shows no relationship with $PM_{2.5}$ concentrations (Fig. 6c). Our measured pH of filtrate ranged from 4.6 to

8.2 with a mean of 5.7 ±1.0, similar to pH of filtrate from $PM_{2.5}$ in Beijing reported by Wang et al. (2005). The measured pH of filtrate shows similar trends with bulk aerosol pH calculated assuming metastable state (Fig. 6c), with a mean value 6.9 ±0.7 in NPD and 5.1 ±0.6 in PD, which suggests that bulk aerosols are in metastable state with moderate acidity in PD. This is also consistent with our estimate that most aerosols are in metastable with a fraction of (74 ±17) % in PD by using Eq. (9) and our cognition that the mixture of major acidic aerosols with minor neutral aerosols would lead to the bulk being acidic. However, as the effective Henry's law constant of SO_2 at pH = 7.6 (stable state) can be 3 orders magnitude higher than that at pH = 4.4 (metastable state in PD) rendering even a small fraction of aerosol at this high pH value being potentially significant active sites for heterogeneous sulfate production during PD.

The main heterogeneous sulfate formation pathways considered include S(IV) oxidation by H_2O_2, O_3, NO_2 and O_2 on acidic microdroplets as proposed by Hung and Hoffmann (2015). Other sulfate formation pathways such as S(IV) oxidation by NO_3 radical, methyl-hydrogenperoxide (MHP), peroxyacetic acid (PAA), and hypohalous acids in aerosol water (Feingold et al., 2002; Walcek and Taylor, 1986; Chen et al., 2017) is thought to be negligible during haze in NCP (Cheng et al., 2016), and thus is not considered here. We estimate the relative importance of these heterogeneous sulfate formation pathways as follows. First, the heterogeneous sulfate production rate via S(IV) oxidation by H_2O_2 ($P_{het,\ S(IV)+H2O2}$) was calculated with the influence of I_s being considered, which has been determined at high I_s in laboratories (Table S3 and S5). Then, the fractional contribution of H_2O_2 oxidation ($f_{het,\ S(IV)+H2O2}$) to overall heterogeneous sulfate production (P_{het}) calculated using apparent γ (see Sect. 2.3) was estimated. Large uncertainties exist in the influence of I_s on the reaction rate constant of S(IV) oxidation by O_3 in aerosol water (Table S3), renders the estimate of its fractional contribution ($f_{het,\ S(IV)+O3}$) to P_{het} from purely chemical kinetic calculations uncertain. Instead, $f_{het,\ S(IV)+O3}$ was estimated using our calculated $f_{het,\ S(IV)+H2O2}$ and $\Delta^{17}O_{het}$ values, on the basis that $\Delta^{17}O(SO_4^{2-}) > 0$ ‰ originates solely from H_2O_2 and O_3 oxidation. Then zero-$\Delta^{17}O$ pathways such as S(IV) oxidation by NO_2 and by O_2 was estimated to be the remaining part ($f_{het,\ zero\text{-}\Delta17O}$). At last, the potential importance of S(IV) oxidation by NO_2 and by O_2 is discussed.

Calculations show that $f_{het,\ S(IV)+H2O2}$ was 4–6 % with a mean of (5 ±1) % under stable aerosol assumptions, and 8–19 % with a mean of (13 ±4) % under metastable state assumptions for PD of all the cases. $f_{het,\ S(IV)+O3}$ was calculated to be 2–47 % with a mean of (22 ±17) % in stable state assumption and 0–47 % with a mean of (21 ±18) % in metastable state assumption. Correspondingly, $f_{het,\ zero\text{-}\Delta17O}$ was the remaining 73 % (47–94 %) in stable assumption, or 66 % (42–81 %) in metastable assumption for PD of all the cases (Fig. 7). Excluding PD of Case II, in which sulfate formation was predominated by in-cloud reactions, our local atmospheric conditions-based calculations suggest zero-$\Delta^{17}O$ pathways such as S(IV) oxidation by NO_2 and/or by O_2 are important for sulfate formation during Beijing haze.

Cheng et al. (2016) suggested that S(IV) oxidation by NO_2 in aerosol water could largely account for the missing sulfate source in 2013 Beijing haze. In their study, the calculated mean aerosol pH is 5.8, while influence of I_s was not taken into

account due to the lack of relevant experimental data. The calculated $P_{het, S(IV)+NO2}$ is highly sensitive to aerosol pH. In our study, when aerosol pH decreased from 7.6±0.1 assuming stable state to 4.7±1.1 assuming metastable state, mean $P_{het, S(IV)+NO2}$ decreased from (6.5±7.7) μg m^{-3} h^{-1} to (0.01±0.02) μg m^{-3} h^{-1} for PD of all the cases (Fig. 7). The former is much larger than our estimate of overall heterogeneous production rate, P_{het} = (2.0±1.1) μg m^{-3} h^{-1}, while the latter is too small. Moreover, the influence of I_s was not considered, which is expected to increase the reaction rate constant of S(IV) oxidation by NO_2 (Cheng et al., 2016). The treatment of aerosols as a bulk quantity, assuming that all aerosols are either in stable or metastable state, or that all aerosol particles have the same pH, may lead to errors in calculating heterogeneous sulfate production rates. As stated in Sect. 2.8, not all aerosols are in metastable state, even though the fractional occurrence of metastable aerosols increases with increasing relative humidity (Rood et al., 1989). Fig. 8a shows that the fraction of metastable aerosols to total aerosols, estimated by using Eq. (9), increases with $PM_{2.5}$ levels. However, when assuming a combination of stable and metastable state aerosol as shown in Eq. (9), $P_{het, S(IV)+NO2}$ increases with $PM_{2.5}$ levels and reaches (0.9±0.7) μg m^{-3} h^{-1} during PD of all the cases (Fig. 8b), much higher than $P_{het, S(IV)+NO2}$ = (0.01±0.02) μg m^{-3} h^{-1} under sole metastable aerosol assumption. This estimate suggests that even though the majority of aerosols may be in metastable state during PD (74 ±17 % in our calculation), the high pH of the minority of aerosols in stable state could render S(IV) oxidation by NO_2 a potentially significant pathway for heterogeneous sulfate production.

Since $P_{het, S(IV)+NO2}$ using calculated aerosol pH assuming metastable state was two orders of magnitude lower than P_{het} during PD, we further examined S(IV) oxidation by O_2 on acidic microdroplets under the metastable state assumption. A laboratory study suggested that SO_2 oxidation by O_2 on acidic microdroplets has a large aqueous-phase reaction rate constant of 1.5×10^6[S(IV)] (M s^{-1}) at pH ≤ 3, a pH range much lower than our calculated pH values. The rate constant was shown to decrease with increasing pH, however, no values of the rate constant at pH > 3 was reported (Hung and Hoffmann, 2015). Figure 7b shows heterogensous sulfate production rate via S(IV) oxidation by O_2 on acidic microdroplets ($P_{het, S(IV)+O2}$) with aerosol liqiud water content calculated assuming metastable state and the aqueous-phase rate constant for pH ≤ 3 being used, even though the calculated aerosol pH is > 3. The estimated $P_{het, S(IV)+O2}$ is 1.5×10^3 to 1.3×10^5 μg m^{-3} h^{-1} with a mean of 2.5×10^4 μg m^{-3} h^{-1} during PD of all cases, which is four order of magnitude larger than P_{het}. This value should be an overestimate due to our calculated bulk aerosol pH predicted in metastable state being 4.4±0.6 during PD and the experimental results of He et al. (2014) and Wang et al. (2016) suggests O_2 oxidation pathway is negligible at higher pH conditions (e.g., on CaO and in NH_4^+ solution). However, some fraction of aerosols may have pH ≤ 3 due to the Kelvin effect (Hung and Hoffmann, 2015), rendering S(IV) oxidation by O_2 on acidic microdroplets a potentially important pathway for heterogeneous sulfate production even if it may occur on only a small fraction of the ambient aerosol.

4 Conclusions

Our study suggests that both in-cloud reactions and heterogeneous reactions can dominate sulfate formation during Beijing haze, with the fractional contribution of f_{cloud} = 68% in Case II and f_{het} = (48±5) % in Case I and III–V. The $\Delta^{17}O$-constrained calculation shows that the heterogeneous sulfate production during haze events in our observation was mainly (66 to 73 % on average) from reactions that result in sulfate with $\Delta^{17}O$ = 0 ‰, e.g., S(IV) oxidation by NO_2 and/or by O_2. S(IV) oxidation by H_2O_2 and O_3 accounted for the rest (27 to 34 %) of heterogeneous sulfate production. However, given the large difference in predicted aerosol pH assuming metastable aerosol state and stable aerosol state (pH = 7.6±0.1 and 4.7±1.1, respectively) and the strong dependence of SO_2 oxidation on aerosol pH, we cannot quantify the relative importance of these two pathways for heterogeneous sulfate production. S(IV) + NO_2 can be the dominant pathway when aerosols are in stable state with pH = 7.6±0.1, while S(IV) + O_2 can take over providing that highly acidic aerosols (pH ≤ 3) exist. To distinguish which of these two mechanisms is more important for sulfate formation during Beijing haze, the heterogeneity of aerosol state and pH should be considered in future studies.

Supplementary Materials

Table S1. Reaction rate expression and constant for SO_2 oxidation by OH in the gas-phase.

Table S2. The daytime average OH concentration.

Table S3. Aqueous-phase reaction rate expressions, rate constants (k) and influence of ionic strength (I_s) on k for sulfate production in aerosol and cloud water.

Table S4. Summary for the input and output of ISORROPIA II model.

Table S5. Calculations of aqueous-phase concentrations, equilibrium constants and influence of ionic strength.

Table S6. Observed $\Delta^{17}O(SO_4^{2-})$ in aerosols or rainwater in mid-latitude areas.

Data availability

All data needed to draw the conclusions in the present study are shown in this paper and/or the Supplementary Materials. For additional data related to this study, please contact the corresponding author (zqxie@ustc.edu.cn).

Author contributions

Z.Q.X. initiated and led the study. P.Z.H. conducted oxygen isotope measurements supervised by B.A. and L.G.. P.Z.H., X.Y.C, S.D.F., H.C.Z., H. K. performed the field experiments and aerosol chemical composition measurements. P.Z.H., B.A., Z.Q.X., L.G., H.S. and Y.F.C. interpreted the data. H.S., Y.F.C. and G.J.Z. involved the discussion of oxidation pathway

calculation. C.L. contributed to the field observation support. P.Z.H. wrote the manuscript with B.A., Z.Q.X. and L.G. inputs. All authors involved the discussion and revision.

Competing interests

The authors declare no competing interests.

Acknowledgments

We thank A. J. Schauer and Q. J. Chen at the University of Washington for help with isotope ratio measurements. Z. Q. Xie acknowledges support from National Key Project of MOST (2016YFC0203302), NSFC (91544013), the Key Project of CAS (KJZD-EW-TZ-G06-01) and the Atmospheric Pollution Control of the Prime Minister (DQGG0104). B. Alexander acknowledges support from NSF AGS 1644998. H. Su acknowledges support from National Key Project of MOST (2017YFC0210104) and NSFC (91644218).

References

Alexander, B., Park, R. J., Jacob, D. J., Li, Q., Yantosca, R. M., Savarino, J., Lee, C., and Thiemens, M.: Sulfate formation in sea‐salt aerosols: Constraints from oxygen isotopes, J. Geophys. Res., 110, D10307, 2005.

Alexander, B., Park, R. J., Jacob, D. J., and Gong, S.: Transition metal‐catalyzed oxidation of atmospheric sulfur: Global implications for the sulfur budget, J. Geophys. Res., 114, D02309, 2009.

Alexander, B., Allman, D., Amos, H., Fairlie, T., Dachs, J., Hegg, D. A., and Sletten, R. S.: Isotopic constraints on the formation pathways of sulfate aerosol in the marine boundary layer of the subtropical northeast Atlantic Ocean, J. Geophys. Res., 117, D06304, 2012.

Bao, H., Thiemens, M. H., Farquhar, J., Campbell, D. A., Lee, C. C.-W., Heine, K., and Loope, D. B.: Anomalous ^{17}O compositions in massive sulphate deposits on the Earth, Nature, 406, 176-178, 2000.

Bian, Y., Zhao, C., Ma, N., Chen, J., and Xu, W.: A study of aerosol liquid water content based on hygroscopicity measurements at high relative humidity in the North China Plain, Atmos. Chem. Phys., 14, 6417-6426, 2014.

Brook, R. D., Rajagopalan, S., Pope, C. A., Brook, J. R., Bhatnagar, A., Diez-Roux, A. V., Holguin, F., Hong, Y., Luepker, R. V., and Mittleman, M. A.: Particulate matter air pollution and cardiovascular disease an update to the scientific statement from the American Heart Association, Circulation, 121, 2331-2378, 2010.

Calhoun, J. A., Bates, T. S., and Charlson, R. J.: Sulfur isotope measurements of submicrometer sulfate aerosol particles over the Pacific Ocean, Geophys. Res. Lett., 18, 1877-1880, 1991.

Chen, Q., Geng, L., Schmidt, J. A., Xie, Z., Kang, H., Dachs, J., Cole-Dai, J., Schauer, A. J., Camp, M. G., and Alexander, B.: Isotopic constraints on the role of hypohalous acids in sulfate aerosol formation in the remote marine boundary layer, Atmos. Chem. Phys., 16, 11433-11450, 2016.

Chen, Q., Schmidt, J. A., Shah, V., Jaeglé, L., Sherwen, T., and Alexander, B.: Sulfate production by reactive bromine: Implications for the global sulfur and reactive bromine budgets, Geophys. Res. Lett., 2017.

Cheng, Y., Zheng, G., Wei, C., Mu, Q., Zheng, B., Wang, Z., Gao, M., Zhang, Q., He, K., and Carmichael, G.: Reactive nitrogen chemistry in aerosol water as a source of sulfate during haze events in China, Sci. Adv., 2, e1601530, 2016.

Cheng, Z., Jiang, J., Fajardo, O., Wang, S., and Hao, J.: Characteristics and health impacts of particulate matter pollution in China (2001–2011), Atmos. Environ., 65, 186-194, 2013.

Clifton, C. L., Altstein, N., and Huie, R. E.: Rate constant for the reaction of nitrogen dioxide with sulfur (IV) over the pH range 5.3-13, Environ. Sci. Technol., 22, 586-589, 1988.

Dubey, M. K., Mohrschladt, R., Donahue, N. M., and Anderson, J. G.: Isotope specific kinetics of hydroxyl radical (OH) with water (H_2O): Testing models of reactivity and atmospheric fractionation, J. Phys. Chem. A, 101, 1494-1500, 1997.

Faloona, I.: Sulfur processing in the marine atmospheric boundary layer: A review and critical assessment of modeling uncertainties, Atmos. Environ., 43, 2841-2854, 2009.

Feingold, G., Frost, G. J., and Ravishankara, A.: Role of NO_3 in sulfate production in the wintertime northern latitudes, J. Geophys. Res., 107, 2002.

Fountoukis, C., and Nenes, A.: ISORROPIA II: a computationally efficient thermodynamic equilibrium model for K^+–Ca^{2+}–Mg^{2+}–NH_4^+–Na^+–SO_4^{2-}–NO_3^-–Cl^-–H_2O aerosols, Atmos. Chem. Phys., 7, 4639-4659, 2007.

Fu, A.: Study on peroxides concentration and its influencing factors in the urban atmosphere, master of engineering, College of Environmental and Resource Sciences, Zhejiang University, Hangzhou, China, 56 pp., 2014.(in Chinese)

Geng, L., Schauer, A. J., Kunasek, S. A., Sofen, E. D., Erbland, J., Savarino, J., Allman, D. J., Sletten, R. S., and Alexander, B.: Analysis of oxygen‐17 excess of nitrate and sulfate at sub‐micromole levels using the pyrolysis method, Rapid Commun. Mass Spectrom., 27, 2411-2419, 2013.

Guo, H., Weber, R. J., and Nenes, A.: High levels of ammonia do not raise fine particle pH sufficiently to yield nitrogen oxide-dominated sulfate production, Sci. Rep., 7, 12109, 2017.

Guo, J., Wang, Y., Shen, X., Wang, Z., Lee, T., Wang, X., Li, P., Sun, M., Collett, J. L., and Wang, W.: Characterization of cloud water chemistry at Mount Tai, China: Seasonal variation, anthropogenic impact, and cloud processing, Atmos. Environ., 60, 467-476, 2012.

Guo, S., Hu, M., Zamora, M. L., Peng, J., Shang, D., Zheng, J., Du, Z., Wu, Z., Shao, M., and Zeng, L.: Elucidating severe urban haze formation in China, P. Natl. Acad. Sci. USA, 111, 17373-17378, 2014.

Harris, E., Sinha, B., van Pinxteren, D., Tilgner, A., Fomba, K. W., Schneider, J., Roth, A., Gnauk, T., Fahlbusch, B., Mertes, S., Lee, T., Collett, J., Foley, S., Borrmann, S., Hoppe, P., and Herrmann, H.: Enhanced Role of Transition Metal Ion Catalysis During In-Cloud Oxidation of SO_2, Science, 340, 727-730, 2013.

He, H., Wang, Y., Ma, Q., Ma, J., Chu, B., Ji, D., Tang, G., Liu, C., Zhang, H., and Hao, J.: Mineral dust and NOx promote the conversion of SO_2 to sulfate in heavy pollution days, Sci. Rep., 4, 4172, 2014.

Hennigan, C., Izumi, J., Sullivan, A., Weber, R., and Nenes, A.: A critical evaluation of proxy methods used to estimate the acidity of atmospheric particles, Atmos. Chem. Phys, 15, 2775-2790, 2015.

Hoffmann, M. R., and Calvert, J. G.: Chemical Transformation Modules for Eulerian Acid Deposition Models: Volume II, the Aqueous-phase Chemistry, Atmospheric Sciences Research Laboratory, Office of Research and Development, US Environmental Protection Agency, 1985.

Holt, B., Kumar, R., and Cunningham, P.: Oxygen-18 study of the aqueous-phase oxidation of sulfur dioxide, Atmos. Environ., 15, 557-566, 1981.

Hung, H.-M., and Hoffmann, M. R.: Oxidation of gas-Phase SO_2 on the surfaces of acidic microdroplets: Implications for sulfate and sulfate radical anion formation in the atmospheric liquid phase, Environ. Sci. Technol., 49, 13768-13776, 2015.

Ibusuki, T., and Takeuchi, K.: Sulfur dioxide oxidation by oxygen catalyzed by mixtures of manganese (II) and iron (III) in aqueous solutions at environmental reaction conditions, Atmos. Environ., 21, 1555-1560, 1987.

Ishino, S., Hattori, S., Savarino, J., Jourdain, B., Preunkert, S., Legrand, M., Caillon, N., Barbero, A., Kuribayashi, K., and Yoshida, N.: Seasonal variations of triple oxygen isotopic compositions of atmospheric sulfate, nitrate, and ozone at Dumont d'Urville, coastal Antarctica, Atmos. Chem. Phys., 17, 3713-3727, 2017.

Jacob, D. J.: Heterogeneous chemistry and tropospheric ozone, Atmos. Environ., 34, 2131-2159, 2000.

Jenkins, K. A., and Bao, H.: Multiple oxygen and sulfur isotope compositions of atmospheric sulfate in Baton Rouge, LA, USA, Atmos. Environ., 40, 4528-4537, 2006.

Jiang, J., Zhou, W., Cheng, Z., Wang, S., He, K., and Hao, J.: Particulate matter distributions in China during a winter period with frequent pollution episodes (January 2013), Aerosol Air Qual. Res., 15, 494-503, 2015.

Lee, C. W., Savarino, J., Cachier, H., and Thiemens, M.: Sulfur (^{32}S, ^{33}S, ^{34}S, ^{36}S) and oxygen (^{16}O, ^{17}O, ^{18}O) isotopic ratios of primary sulfate produced from combustion processes, Tellus B, 54, 193-200, 2002.

Lee, Y. N., and Schwartz, S. E.: Kinetics of oxidation of aqueous sulfur (IV) by nitrogen dioxide, in: Kinetics of oxidation of aqueous sulfur (IV) by nitrogen dioxide, Precipitation scavenging, dry Deposition and resuspension, California, 1982, 453-470, 1983.

Legrand, M., Hammer, C., De Angelis, M., Savarino, J., Delmas, R., Clausen, H., and Johnsen, S. J.: Sulfur‐containing species (methanesulfonate and SO4) over the last climatic cycle in the Greenland Ice Core Project (central Greenland) ice core, J. Geophys. Res., 102, 26663-26679, 1997.

Legrand, M., and Mayewski, P.: Glaciochemistry of polar ice cores: A review, Rev. Geophys., 35, 219-243, 1997.

Li, L., Chen, Z., Zhang, Y., Zhu, T., Li, J., and Ding, J.: Kinetics and mechanism of heterogeneous oxidation of sulfur dioxide by ozone on surface of calcium carbonate, Atmos. Chem. Phys., 6, 2453-2464, 2006.

Li, X., Bao, H., Gan, Y., Zhou, A., and Liu, Y.: Multiple oxygen and sulfur isotope compositions of secondary atmospheric sulfate in a mega-city in central China, Atmos. Environ., 81, 591-599, 2013.

Lin, M., Biglari, S., Zhang, Z., Crocker, D., Tao, J., Su, B., Liu, L., and Thiemens, M. H.: Vertically uniform formation pathways of tropospheric sulfate aerosols in East China detected from triple stable oxygen and radiogenic sulfur isotopes, Geophys. Res. Lett., 2017.

Liu, M., Song, Y., Zhou, T., Xu, Z., Yan, C., Zheng, M., Wu, Z., Hu, M., Wu, Y., and Zhu, T.: Fine Particle pH during Severe Haze Episodes in Northern China, Geophys. Res. Lett., 2017.

Liu, X., and Millero, F. J.: The solubility of iron hydroxide in sodium chloride solutions, Geochim. Cosmochim. Acta, 63, 3487-3497, 1999.

Luz, B., and Barkan, E.: The isotopic ratios $^{17}O/^{16}O$ and $^{18}O/^{16}O$ in molecular oxygen and their significance in biogeochemistry, Geochim. Cosmochim. Acta, 69, 1099-1110, 2005.

Martin, L. R., and Hill, M. W.: The iron catalyzed oxidation of sulfur: Reconciliation of the literature rates, Atmos. Environ., 21, 1487-1490, 1967.

Matsuhisa, Y., Goldsmith, J. R., and Clayton, R. N.: Mechanisms of hydrothermal crystallization of quartz at 250 ℃ and 15 kbar, Geochim. Cosmochim. Acta, 42, 173-182, 1978.

McArdle, J. V., and Hoffmann, M. R.: Kinetics and mechanism of the oxidation of aquated sulfur dioxide by hydrogen peroxide at low pH, J. Phys. Chem., 87, 5425-5429, 1983.

Meng, Z., Lin, W., Jiang, X., Yan, P., Wang, Y., Zhang, Y., Jia, X., and Yu, X.: Characteristics of atmospheric ammonia over Beijing, China, Atmos. Chem. Phys., 11, 6139-6151, 2011.

Rood, M., Shaw, M., Larson, T., and Covert, D.: Ubiquitous nature of ambient metastable aerosol, Nature, 337, 537-539, 1989.

Savarino, J., and Thiemens, M. H.: Analytical procedure to determine both $\delta^{18}O$ and $\delta^{17}O$ of H_2O_2 in natural water and first measurements, Atmos. Environ., 33, 3683-3690, 1999.

Savarino, J., Lee, C. C., and Thiemens, M. H.: Laboratory oxygen isotopic study of sulfur (IV) oxidation: Origin of the mass‐independent oxygen isotopic anomaly in atmospheric sulfates and sulfate mineral deposits on Earth, J. Geophys. Res., 105, 29079-29088, 2000.

Savarino, J., Alexander, B., Darmohusodo, V., and Thiemens, M. H.: Sulfur and oxygen isotope analysis of sulfate at micromole levels using a pyrolysis technique in a continuous flow system, Anal. Chem., 73, 4457-4462, 2001.

Seinfeld, J. H., and Pandis, S. N.: Atmospheric chemistry and physics: From air pollution to climate change, John Wiley & Sons, New Jersey, 2006.

Shen, C. H., and Rochelle, G. T.: Nitrogen dioxide absorption and sulfite oxidation in aqueous sulfite, Environ. Sci. Technol., 32, 1994-2003, 1998.

Shen, X., Lee, T., Guo, J., Wang, X., Li, P., Xu, P., Wang, Y., Ren, Y., Wang, W., and Wang, T.: Aqueous phase sulfate production in clouds in eastern China, Atmos. Environ., 62, 502-511, 2012.

Sofen, E., Alexander, B., Steig, E., Thiemens, M., Kunasek, S., Amos, H., Schauer, A., Hastings, M., Bautista, J., and Jackson, T.: WAIS Divide ice core suggests sustained changes in the atmospheric formation pathways of sulfate and nitrate since the 19th century in the extratropical Southern Hemisphere, Atmos. Chem. Phys., 14, 5749-5769, 2014.

Sun, Y., Zhuang, G., Tang, A., Wang, Y., and An, Z.: Chemical characteristics of $PM_{2.5}$ and PM_{10} in haze-fog episodes in Beijing, Environ. Sci. Technol., 40, 3148-3155, 2006.

Vicars, W. C., and Savarino, J.: Quantitative constraints on the 17O-excess ($\Delta^{17}O$) signature of surface ozone: Ambient measurements from 50 ºN to 50 ºS using the nitrite-coated filter technique, Geochim. Cosmochim. Acta, 135, 270-287, 2014.

Walcek, C. J., and Taylor, G. R.: A theoretical method for computing vertical distributions of acidity and sulfate production within cumulus clouds, J. Atmos. Sci., 43, 339-355, 1986.

Wang, G., Zhang, R., Gomez, M. E., Yang, L., Zamora, M. L., Hu, M., Lin, Y., Peng, J., Guo, S., and Meng, J.: Persistent sulfate formation from London Fog to Chinese haze, P. Natl. Acad. Sci. USA, 113, 13630-13635, 2016.

Wang, Y., Zhuang, G., Tang, A., Yuan, H., Sun, Y., Chen, S., and Zheng, A.: The ion chemistry and the source of $PM_{2.5}$ aerosol in Beijing, Atmos. Environ., 39, 3771-3784, 2005.

Wang, Y., Zhang, Q., Jiang, J., Zhou, W., Wang, B., He, K., Duan, F., Zhang, Q., Philip, S., and Xie, Y.: Enhanced sulfate formation during China's severe winter haze episode in January 2013 missing from current models, J. Geophys. Res., 119, 10425-10440, 2014.

Ye, P., Xie, Z., Yu, J., and Kang, H.: Spatial distribution of methanesulphonic acid in the Arctic aerosol collected during the Chinese Arctic Research Expedition, Atmosphere, 6, 699-712, 2015.

Zheng, B., Zhang, Q., Zhang, Y., He, K., Wang, K., Zheng, G., Duan, F., Ma, Y., and Kimoto, T.: Heterogeneous chemistry: a mechanism missing in current models to explain secondary inorganic aerosol formation during the January 2013 haze episode in North China, Atmos. Chem. Phys., 15, 2031-2049, 2015a.

Zheng, G., Duan, F., Su, H., Ma, Y., Cheng, Y., Zheng, B., Zhang, Q., Huang, T., Kimoto, T., and Chang, D.: Exploring the severe winter haze in Beijing: the impact of synoptic weather, regional transport and heterogeneous reactions, Atmos. Chem. Phys., 15, 2969-2983, 2015b.

Figures and Tables

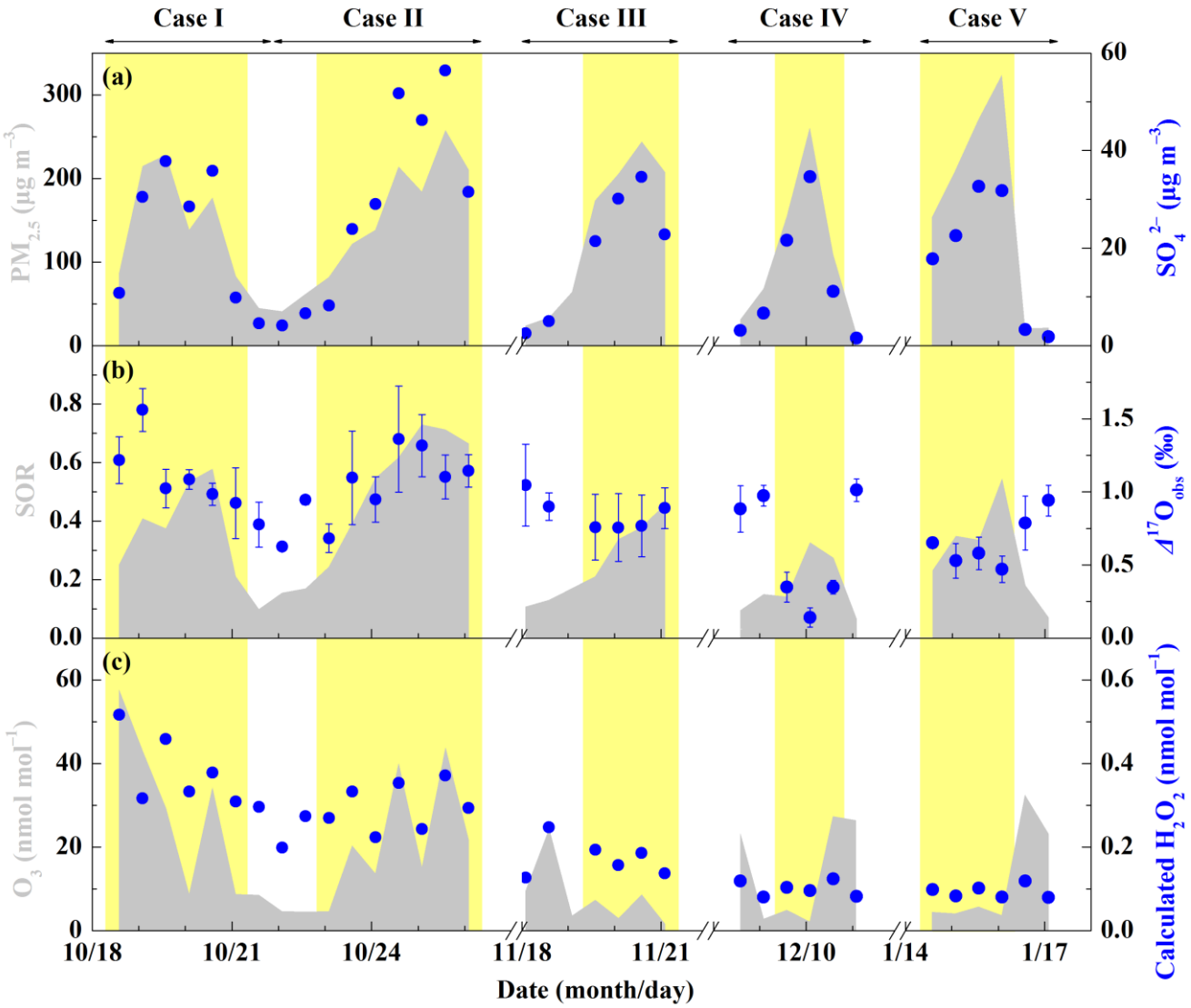

Figure 1. Characteristics of haze events in Beijing (October 2014–January 2015). **(a)** Temporal evolution of $PM_{2.5}$ and SO_4^{2-} concentrations. **(b)** Temporal evolution of sulfur oxidation ratio (SOR, which equals to SO_4^{2-} molar concentration divided by the sum of SO_4^{2-} and SO_2 molar concentration) and observed $\Delta^{17}O(SO_4^{2-})$ ($\Delta^{17}O_{obs}$). **(c)** Temporal evolution of observed O_3 and calculated H_2O_2. The error bar of $\Delta^{17}O_{obs}$ in (b) is ±1σ of replicate measurements (n = 2–4) of each sample. The light

yellow shaded area indicates polluted days (PD, $PM_{2.5} \geq 75$ μg m^{-3}). Data used here are 12h-averaged values, corresponding with filter samples.

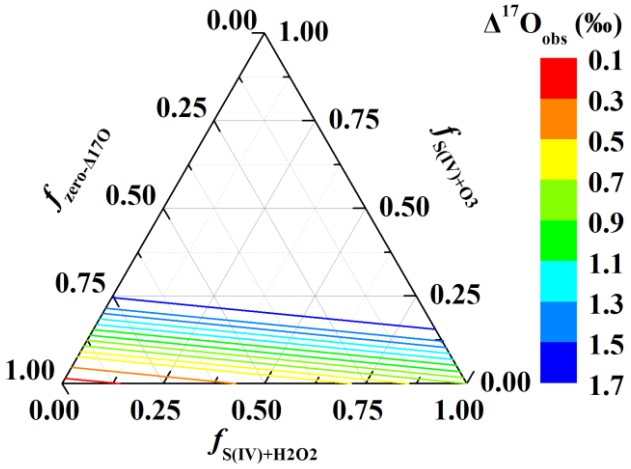

Figure 2. Ternary diagram of possible fractional contribution of different pathways to total sulfate production directly estimated from $\Delta^{17}O_{obs}$. The colored lines are contour lines of $\Delta^{17}O_{obs}$, representing possible fractional contribution of sulfate formation via O_3 ($f_{S(IV)+O3}$) and H_2O_2 ($f_{S(IV)+H2O2}$) oxidation or zero-$\Delta^{17}O$ processes ($f_{zero\text{-}\Delta17O}$) such as primary sulfate, secondary sulfate formed via OH oxidation, NO_2 oxidation and O_2 oxidation. $f_{S(IV)+H2O2}$ is in the range of 0 to min{$\Delta^{17}O_{obs}$/0.7‰, (6.5‰–$\Delta^{17}O_{obs}$)/5.8‰}, $f_{S(IV)+O3} = (\Delta^{17}O_{obs}–0.7‰\times f_{S(IV)+H2O2})/6.5‰$ and $f_{zero\text{-}\Delta17O} = (6.5‰–\Delta^{17}O_{obs}–5.8‰\times f_{S(IV)+H2O2})/6.5‰$. See equation 6 and its caption in Sect. 2.7 for details.

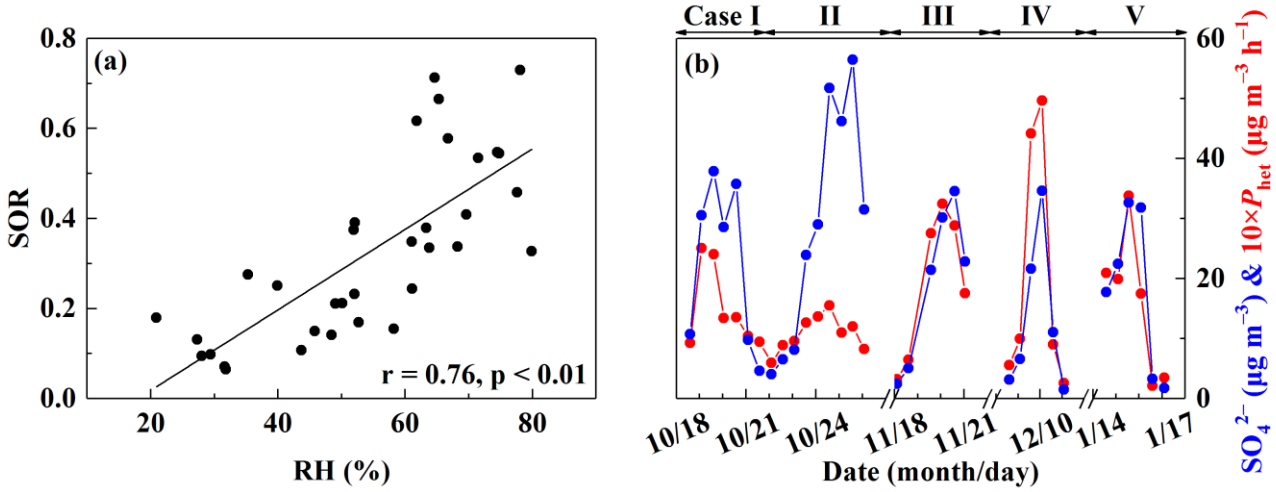

Figure 3. The relationship between relative humidity (RH) and SOR **(a)** and time series of overall heterogeneous sulfate production (P_{het}) along with SO_4^{2-} concentrations **(b)**. The black line in (a) is linear least-squares fitting line.

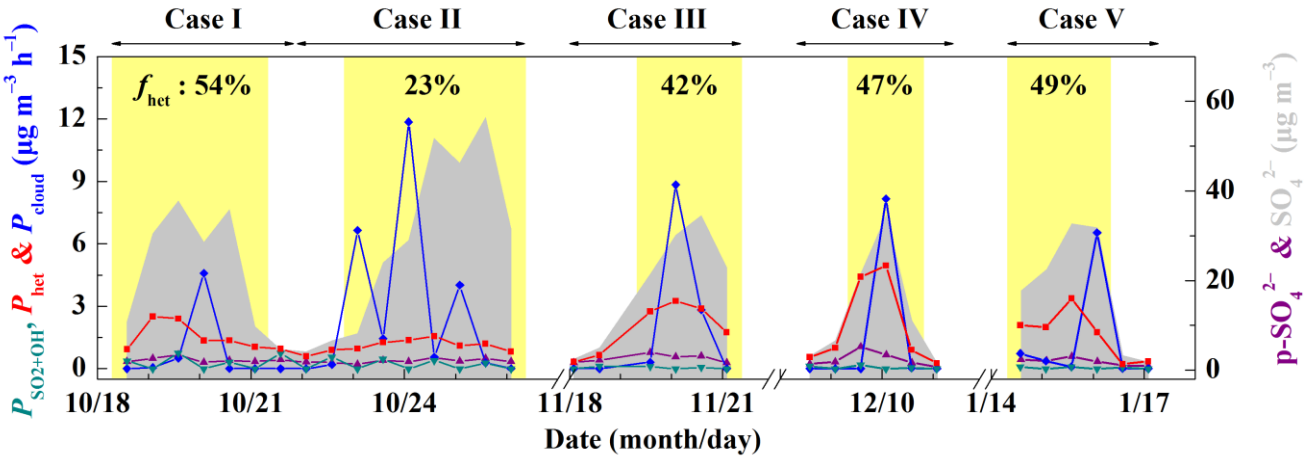

585

586 **Figure 4.** Estimate of different sulfate production pathways. Time series of estimated sulfate production rate via OH
587 oxidation in the gas-phase (P_{SO2+OH}), overall heterogeneous reactions on aerosols (P_{het}) and in-cloud reactions (P_{cloud}) and
588 concentrations of primary sulfate (p-SO_4^{2-}) and observed sulfate. f_{het} represents the fraction of overall heterogeneous sulfate
589 production to total sulfate production during PD of each Case. The light yellow shaded area indicates polluted days (PD,
590 $PM_{2.5} \geq 75$ μg m^{-3}). Data used here are 12h-averaged values, corresponding with filter samples.

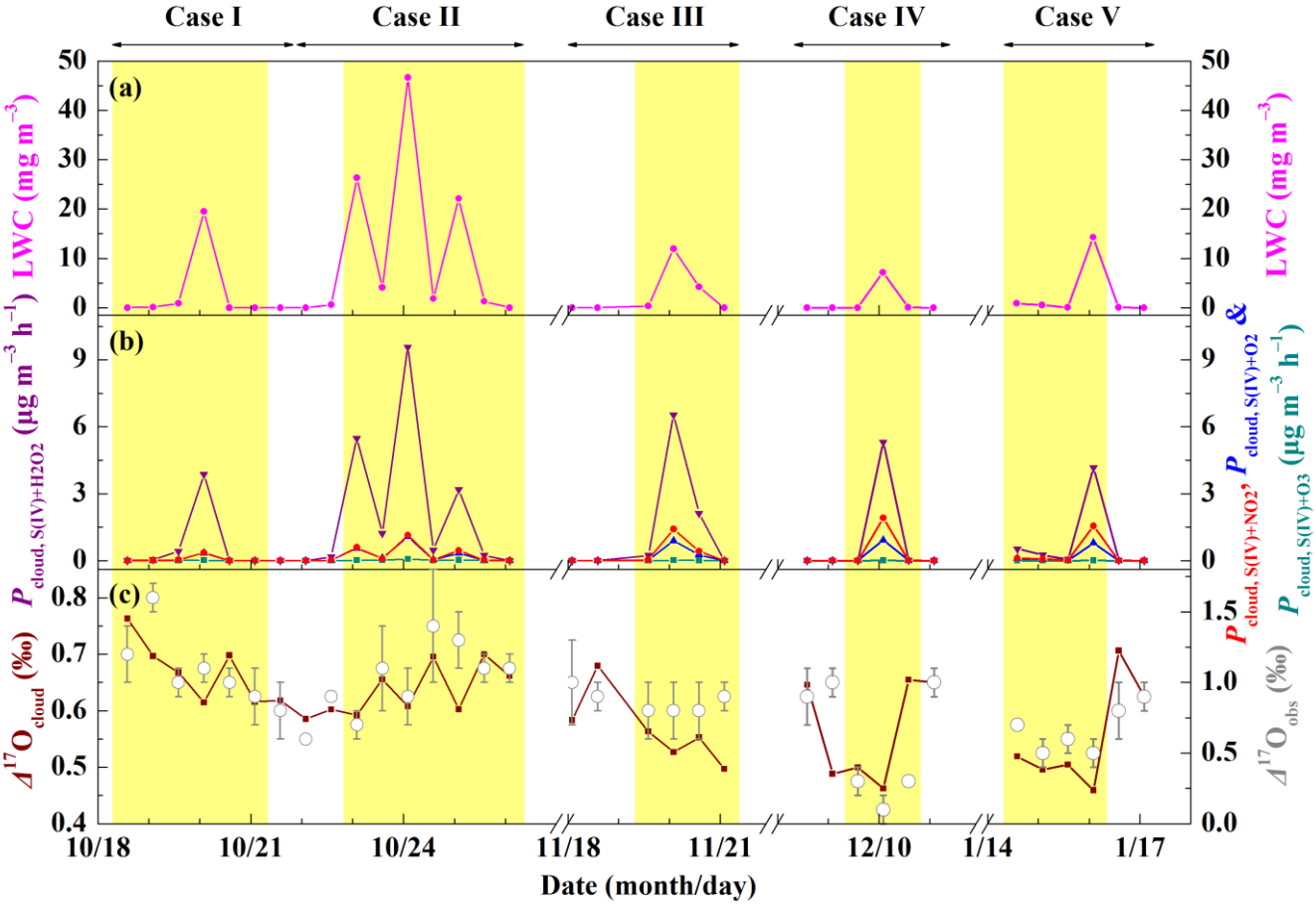

591

592 **Figure 5.** Temporal evolution of cloud liquid water content (LWC, **a**), in-cloud sulfate production rate via S(IV) oxidation by
593 H_2O_2, O_3, NO_2 and O_2 initiated by TMIs (denoted as $P_{cloud, S(IV)+H2O2}$, $P_{cloud, S(IV)+O3}$, $P_{cloud, S(IV)+NO2}$ and $P_{cloud, S(IV)+O2}$, respectively,

b) and estimated $\Delta^{17}O$ of sulfate produced in clouds ($\Delta^{17}O_{cloud}$, **c**). The light yellow shaded area indicates polluted days (PD, $PM_{2.5} \geq 75$ μg m^{-3}). Data used here are 12h-averaged values, corresponding with filter samples.

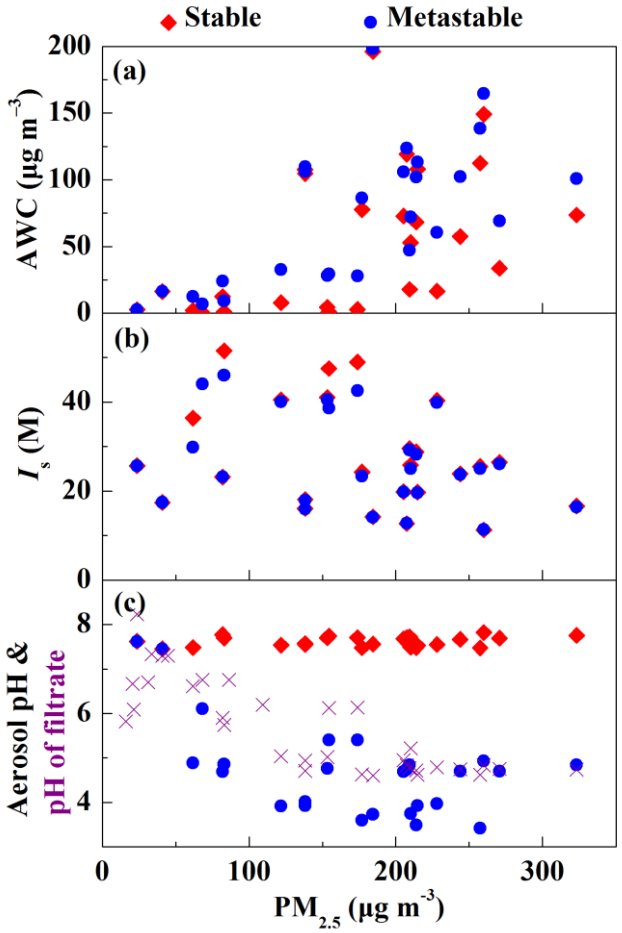

Figure 6. Aerosol parameters during Beijing haze. The aerosol liquid water content (AWC, **a**), ionic strength (I_s, **b**) and aerosol pH (**c**) was predicted by ISORROPIA II assuming stable aerosol state and metastable aerosol state. The pH of filtrate was measured by an ion activity meter.

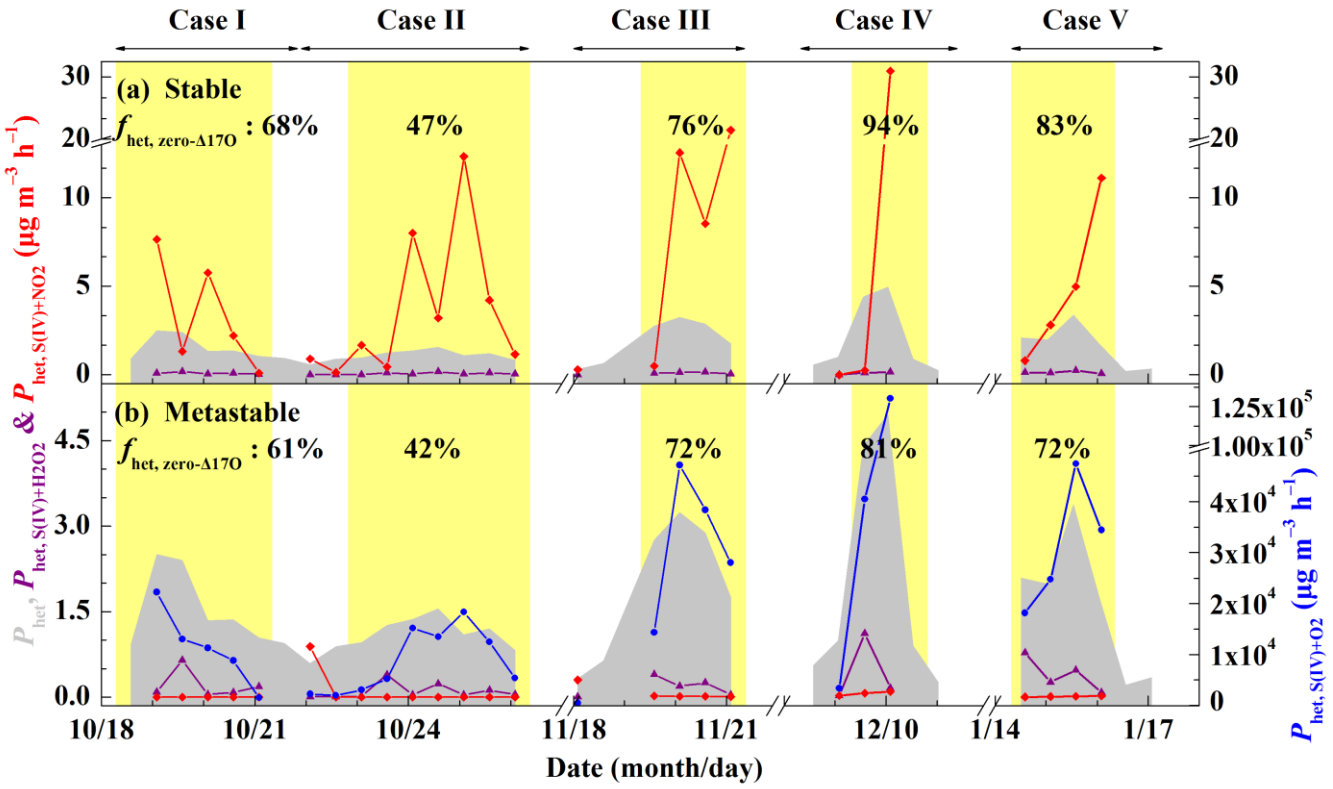

Figure 7. Estimate of heterogeneous sulfate production pathways. Time series of overall heterogeneous sulfate production rate (P_{het}), heterogeneous sulfate production rate in aerosol water via H_2O_2 ($P_{het, S(IV)+H2O2}$) and NO_2 ($P_{het, S(IV)+NO2}$) under stable **(a)** and metastable **(b)** aerosol assumption. $P_{het, S(IV)+O2}$ in (b) represents heterogeneous sulfate production rate via SO_2 oxidation by O_2 via a radical chain mechanism on acidic microdroplets. $f_{het, zero-\Delta17O}$ represents the fraction of heterogeneous reactions that result in sulfate with zero-$\Delta^{17}O$, such as S(IV) oxidation by NO_2 and O_2, to the overall heterogeneous sulfate production during PD of each case with the constraint of $\Delta^{17}O(SO_4^{2-})$ (see the main text for details). In calculating $P_{het, S(IV)+H2O2}$, the influence of I_s was considered. In calculating $P_{het, S(IV)+NO2}$, and $P_{het, S(IV)+O2}$ the influence of I_s was not considered due to the lack of experimental data about the influence of I_s. $P_{het, S(IV)+O2}$ was calculated using the aqueous-phase rate constant for pH ≤ 3 due to the lack of rate constant information at pH > 3. The light yellow shaded area indicates polluted days (PD, $PM_{2.5} \geq 75$ μg m^{-3}). Data used here are 12h-averaged values, corresponding with filter samples.

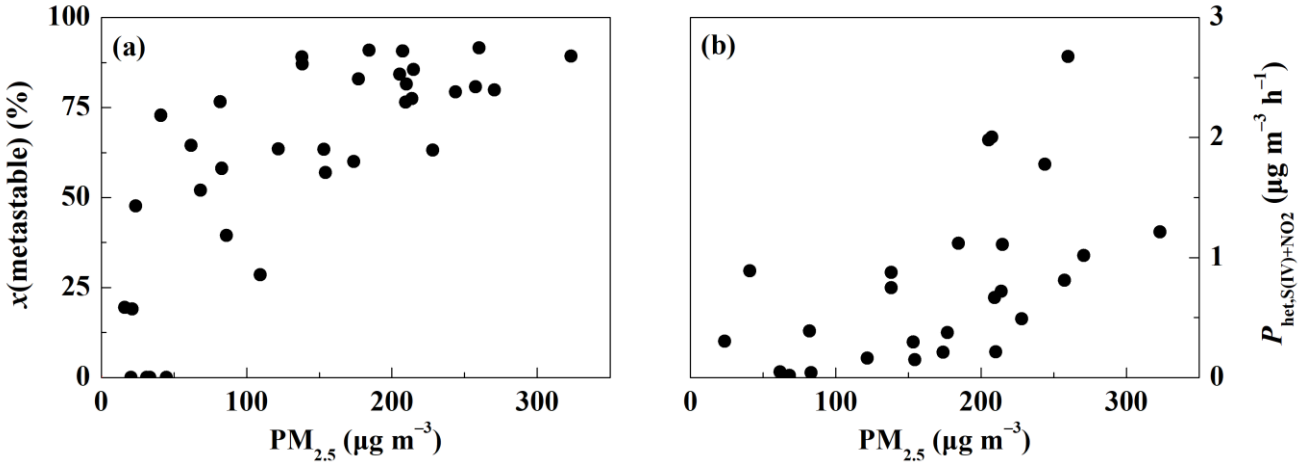

612 **Figure 8.** The estimated fraction of metastable aerosol to total aerosol (x(metastable), **a**) using Eq. (9) and heterogeneous

613 sulfate production rate from S(IV) oxidation by NO_2 assuming a combination of metastable and stable state ($P_{het, S(IV)+NO2}$, **b**) as

614 $P_{het, S(IV)+NO2} = x(\text{metastable}) \times P_{het, S(IV)+NO2, metastable} + (100\ \% - x(\text{metastable})) \times P_{het, S(IV)+NO2, stable}$.

615 **Table 1.** Sulfate isotope assumptions.

Sulfate formation pathways	$\Delta^{17}O(SO_4^{2-})$ (‰)
SO_2 + OH	0
S(IV) + H_2O_2	0.7
S(IV) + O_3	6.5
S(IV) + NO_2	0
S(IV) + O_2	0
Primary sulfate	0

616 **Table 2.** Estimated fractional contribution of different sulfate production pathways during Beijing haze.

PD of case	f_p (%)[a]	f_{het} (%)	f_{cloud} (%)	f_{SO2+OH} (%)
I	9	54	29	8
II	6	23	68	3
III	11	41	47	1
IV	15	47	37	1
V	9	49	41	1

617 [a] f_p, f_{het}, f_{cloud}, and f_{SO2+OH} respectively represents fractional contribution from primary sulfate, heterogeneous reactions,

618 in-cloud reactions and gas-phase pathway.